Two-Beam Coupling between Filament-Forming Beams in Air

A. C. Bernstein, M. McCormick, G. M. Dyer, J. C. Sanders, and T. Ditmire
Department of Physics, University of Texas at Austin, Texas 78712, USA
(Received 29 September 2008; published 24 March 2009)

We experimentally demonstrate two-beam coupling between nearly identical filament-forming beams intersecting in air. A 7% amplification of one beam occurs at the energy expense of the other in a single interaction, controllable by adjusting their relative delay by tens of femtoseconds. The data are consistent with the impulsive Raman nonlinear response of the air molecules as the coupling mechanism. The filament conical emission is controllably enhanced or suppressed by the interaction, indicating that two-beam coupling may be an effective means for filament regeneration and control.

DOI: 10.1103/PhysRevLett.102.123902 PACS numbers: 42.65.Jx, 42.50.Md, 42.65.Re, 42.65.Sf

Optical filaments formed from intense ultrashort pulses in air are studied as interesting phenomena in themselves [1], and for use in a variety of applications including few-cycle pulse generation [2], lightning and discharge triggering and guiding [3,4], remote-sensing [5,6], and even power-delivery [7]. Filaments appear as narrow beam features with extended propagation which result from a balance between beam self-focusing and the defocusing due to ionization. In air this balance occurs at diameters around 100 μm [1] when portions of the beam have attained an intensity above the air ionization threshold, $I_{\mathrm{th}} = 3 \times 10^{13}$ W/cm^2 [1,8].

The potential applications of filaments in atmosphere have driven efforts to control their propagation, with emphasis on the onset [9] and propagation distances [10,11]. Until recently [12,13], techniques to lengthen filament propagation depended on changing the pulse initial conditions before launch. It would be especially desirable to control filament propagation by modifying their characteristics in flight, as would be possible using intersecting beams.

Two-beam coupling (TBC) is a candidate process for this level of filament control. TBC occurs when the interference pattern of two beams produces a spatial material grating via the nonlinear index of refraction, n_2, that acts as a diffraction grating on the beams. A material with a real-valued nonlinear index forms a purely refractive grating that, under ideal conditions, can affect an energy exchange between beams without affecting their phases [14]. For an energy exchange to take place the nonlinear material response must have a significant noninstantaneous component. Air has a real-valued nonlinearity with such a delayed component having a decay time on the order of 100 fs.

In this Letter we present experimental results on the interaction of two nearly identical beams that were either below or above the threshold for forming filaments. The beams intersected such that one beam was amplified in air at an energy cost to the other beam. This study of noncollinear beams in air clearly shows controlled interactions distinct from those studied using parallel-going beams [15–17], or where the simulation neglects the delayed nonlinear response of air [18], or even where intersecting pulses are consistent with filament formation but do not overlap in time [12,13]. While degenerate four-wave mixing experiments have been performed on atmospheric pressure N_2 and O_2 [19], we present here measurements of the delayed nonlinear susceptibility of air using the two-beam coupling technique.

For these experiments we used the THOR laser, a chirp-pulsed amplified Ti:sapphire laser capable of producing pulses with a FWHM duration of 42-fs at an energy of 700 mJ ($\pm$5% RMS shot-to-shot), and at a wavelength of 800 nm. We took extensive measures to form our filaments from beams with nearly identical launch conditions, as the propagation in air of intense ultrashort pulses has been shown to be quite sensitive to initial conditions [20,21]. First, the amplified beam was passed through serrated apertures placed side-by-side, and then passed through the same spatial filter and temporal compressor combination. This produced parallel-going ultrashort pulses with nearly Gaussian spatial profiles with a FWHM diameter of 3 mm. Autocorrelation measurements were made for each compressor setting to determine the initial pulse duration. As shown in Fig. 1, the compressed pulses were routed to a 5-m f.l. mirror followed by beam-steering mirrors for each beam. The filaments were crossed with a half-angle of 0.3°. Beam tubes were not used in the experiments and all normal room air handlers were operating, resulting in air paths with some turbulence.

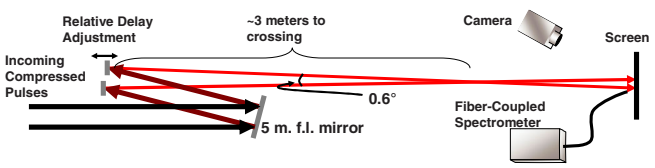

FIG. 1 (color online). Schematic of experimental setup.

The laser energy in these experiments was varied to explore two-beam coupling at intensities either below or above filamentation. The presence of a filament was determined using burn paper to record the transverse beam shape. At the higher intensities filaments formed with lengths of about 1.6 m, much greater than the 15 cm interaction length of the beams. The expanding beams hit a white paper screen placed 1.8 m after the beam crossing and were imaged by a CCD camera. Neutral-density filters in front of the camera attenuated the light to below saturation levels. A computer-controlled encoded motorized stage adjusted the relative delay (see Fig. 1) of beam 1 (B1) relative to beam 2 (B2), enabling femtosecond-scale time-resolved data. In order to take statistically significant data, 10-20 shots were taken at each motor position. A fiber-coupled spectrometer measured the spatially averaged spectrum of one of the beams, and was recorded with each shot along with the beam image, laser energy, and motor position.

To demonstrate the TBC process occurring in air, initial experiments were conducted with the laser intensity below that necessary to form filaments, so that ionization was not present during the beam interaction. The beam energy was 0.85 mJ and pulses were initially positively chirped to a FWHM duration of 270 fs. Each CCD image contained both beams and was processed by summing the pixels of B1 to the value S_1, and the pixels of B2 to the value S_2. A typical resulting TBC signal is plotted in Fig. 2, calculated as $S = (S_1 - S_2)/(S_1 + S_2)$, with each point corresponding to a single laser shot. For beams of initially identical energy, S represents the percent of energy gained by B1 at the expense of B2. In Fig. 2 the data are presented as a function of τ, the amount of time B1 is delayed relative to B2. The black solid line of Fig. 2 is an average taken at each delay (averaging 10–20 shots). The data have been offset to compensate for B2 having about 5% more initial energy than B1, and the zero delay has been defined as the central zero crossing of the averaged signal.

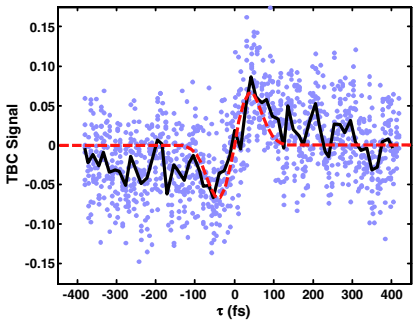

FIG. 2 (color online). Two-beam coupling signal vs time-delay for a positively-chirped pulse of 270 fs, 0.85 mJ, that does not have the intensity to produce filaments. The black line is the average value at each delay position. The red dashed line is a fit calculated with $n_{2,d} = 5 \times 10^{-19}$ cm^2/W using a model described in the text.

The result in Fig. 2 indicates that when the pulses overlap temporally, the trailing pulse obtains energy from the leading pulse, with 270 fs pulses exchanging 7% energy at the peaks. It is important to note that the total energy, $S_1 + S_2$, did not deviate over the range of the scan, indicating that signal S truly represents an energy *exchange*.

The form of the calculated signal, S, of Fig. 2 is that of a typical TBC signal for a material with a positive nonlinear index of refraction in which light is scattered from the beam of higher frequency to that of lower frequency [14,22]. A closed-form solution for the TBC signal exists for the refractive case where the interacting pulses are temporally Gaussian, and the nonlinearity has an exponential response $e^{-(t/\tau_{\rm nl})}$ for $t > 0$ and is zero for $t < 0$, and $\tau_{\rm nl}$ is the nonlinearity decay time. The TBC signal in this case has the form

$$S(\tau) \propto \frac{\Omega(\tau)\tau_{\rm nl}}{1 + [\Omega(\tau)\tau_{\rm nl}]^2}, \tag{1}$$

where $\Omega(\tau) = \omega_1(t - \tau) - \omega_2(t)$ is the frequency difference of the two pulses. As in Refs. [22,23], the frequency difference of our two beams is derived from a relative delay existing between two nearly identical chirped pulses. As our pulses have a positive chirp, instantaneously B1 has a lower frequency than B2 for $\tau > 0$, and, as Fig. 2 shows, gains energy at the expense of B2.

As a further verification of TBC as the relevant nonlinear mechanism, we recorded the pulse interaction resulting from *negatively* chirped pulses of 179 fs FWHM duration, also taken at low energy (0.85 mJ) and below the intensity required for ionization. It is reasonable to assume that the imposed negative chirp overwhelmed any positive chirp accumulated through self-phase modulation while propagating to the interaction region. Equation (1) indicates that a change in chirp should change the sign of S. Indeed the data in Fig. 3 have an opposite sign to the data sets of Fig. 2. This confirms that the energy transfer between pulses depends on their instantaneous relative frequency, and not merely on the time ordering of the pulses.

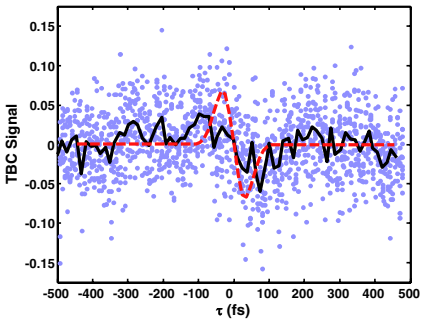

FIG. 3 (color online). Same as Fig. 2, but with an oppositely (negative) chirped pulse of duration 179 fs. The sign of the signal has changed compared to Fig. 2. It is fit with $n_{2,d} = 5 \times 10^{-19}$ cm^2/W.

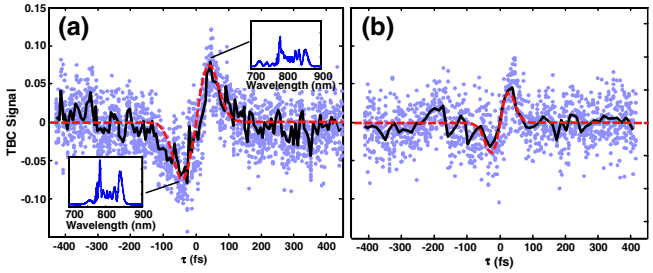

FIG. 4 (color online). Same layout as Fig. 2, but here the pulses are (a) 1.9 mJ, 270 fs, curve fit with $n_{2,d} = 2.5 \times 10^{-19}$ cm^2/W and (b) 0.85 mJ, 90 fs, curve fit with $n_{2,d} = 5 \times 10^{-19}$ cm^2/W. Both data sets have the intensity to produce filaments. Insets: Spatially averaged spectra showing greater modulation of B1 at its largest energy (top spectrum) relative to its smallest energy (bottom spectrum). The spectra are scaled identically.

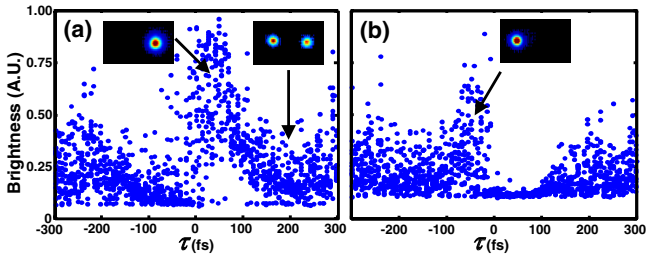

FIG. 5 (color online). Plot of conical emission for the two beams as a function of relative delay. Part (a) shows the conical emission of B1, part (b) shows conical emission of B2. The conical emission of one beam is enhanced when that of the other beam is suppressed.

We additionally demonstrate that more powerful filament-forming beams can undergo the energy exchange. Figure 4 shows data obtained using pulses with intensities to produce filaments on every shot. Figure 4(a) shows data taken with pulses positively chirped to 270 fs with an energy of 1.9 mJ. These data are nearly identical to that shown in Fig. 2, indicating no significant affect of the filament plasma on the energy exchange; again, a measured energy exchange of around 7% takes place, for delays at around $+30$ and -30 fs. The insets are of the spatially averaged spectra, plotted on the same vertical scale, showing that as B1 is amplified it experiences an enhanced nonlinear propagation, as evidenced by greater spectral modulation. Figure 4(b) shows data taken with pulses positively chirped to 90-fs with an energy of 0.85 mJ, and demonstrates an energy exchange of 5%. In addition to a reduced magnitude, Fig. 4(b) shows that 90 fs duration pulses produce a shorter signal temporal width when compared to the 270 fs pulse of Figs. 2 and 4(a). It is important to note that the TBC signal survives in the presence of the filament and, like the lower intensity data, its sign can only be consistent with a positive change of index [14,22], and not with a negative index change that accompanies ionization. This means that plasma generation is an insignificant coupling mechanism at these time scales despite its presence in these beams. This is expected as the interaction volume of the ionized beam regions is no more than one-tenth that of the overall beam.

As a measure of the effect the energy exchange has on filament propagation, we measured filament conical emission by filtering the light scattered from the screen to the CCD with an 800-nm blocking filter. We again positively chirped our pulses to a duration of 270-fs, and set the pulses to an energy of 1.4 mJ. Images in false-color (online) are shown as insets in Fig. 5, with their relevant delays indicated. One image in Fig. 5(a) corresponds to a delay of $+200$ fs, and shows a weak conical emission for both beams where the pulses do not temporally overlap. The other inset of Fig. 5(a) shows the filament conical emission at a delay of $\tau = +17$ fs, where the visible conical emission of B1 is enhanced and that of B2 is reduced to nearly the CCD noise level. The image in Fig. 5(b) shows that the opposite is true at $\tau = -17$ fs. The graphs in Fig. 5 are derived from such images to represent the brightness of B1 [plot of Fig. 5(a)] and B2 [plot of Fig. 5(b)] as a function of τ, calculated by separately summing the pixel-values of B1 and B2 for each image. For $\tau < 0$, B1 has an enhanced conical emission and is temporally behind B2, which has reduced conical emission. For $\tau > 0$ the opposite is true. It is noteworthy that despite the complexity of its formation and propagation, the beam filaments are still reliably controlled by the delay adjustment. It is likely that energy exchange takes place largely in the portion of the beam surrounding the ionization filament, or the "reservoir." Coupling to the filament is then enabled by the reservoir acting as an energy supply to sustain the filament [24,25].

Unlike the decaying exponential assumed as the temporal response used to arrive at Eq. (1), air has a temporal response function, $R(t)$, calculable from quantum-mechanical considerations of N_2 and O_2 molecular rotations, which are made coherent through impulsive stimulation of their Raman-active modes [26]. As the molecules align ($R(t) > 0$) and antialign ($R(t) < 0$) relative to the laser polarization, the light experiences a greater or lesser nonlinear index such that we have the overall nonlinear response:

$$n_2(t) = I(t)n_{2,e} + n_{2,d}\int_{-\infty}^{t} R(t')I(t - t')dt', \qquad (2)$$

where $n_{2,e}$ is the near-instantaneous electronic nonlinear index, $n_{2,d}$ is the delayed nonlinear response coefficient, $I(t)$ is the temporal pulse profile, and $R(t)$ has unity amplitude. It has been experimentally determined that $n_{2,e} \approx n_{2,d}$ [26]. It is the delayed component only that is relevant to the observed energy exchange [14].

To calculate the expected TBC signal S, shown as red dashed lines in Figs. 2–4, we use the treatment of Ref. [27],

which uses electrostatic units. Taking $R(t)$ as purely real, the signal S becomes

$$S(\tau) = \kappa \frac{\sqrt{\pi}\tau_p}{I_0^2} B_{xxxx} \Big\{ -\mathrm{Im}\Big[\int_{-\infty}^{\infty} dt\, u^*(t-\tau)u(t) \times \int_{-\infty}^{t} dt' R(t-t')u(t'-\tau)u^*(t') \Big] \Big\}, \quad (3)$$

where τ_p is the pulse duration, $u(t)$ is the time-dependent electric field, and $I_0 = \int_{-\infty}^{+\infty} |u(t)|^2 dt$. B_{xxxx} is the delayed nonlinear contribution to the third-order susceptibility of air for the linear and parallel-polarized incident beams. The value $\kappa = 24\pi k L_{\mathrm{eff}} E_p/(w_p^2 c \tau_0)$, where $k = 2\pi/\lambda_l$ is the wave number for the central laser wavelength (λ_l) in vacuum, L_{eff} is the effective propagation length (15 cm), E_p is the pulse energy, c is the speed of light. The Gaussian beam-radius w_p at the interaction region was estimated to be 0.68 mm, obtained by imaging the beams on a screen at their crossing point. Equation (3) assumes that the interacting pulses are of equal amplitude, polarization, pulse duration, and diameter.

The dashed red lines in Figs. 2, 3, and 4(b) were calculated using the relevant pulse durations and energies in Eq. (3), and with a fit of $B_{xxxx} = 300$ cm^3/erg-sec as the only adjusted parameter. This obtained a nonlinear susceptibility value of [27]

$$\chi^{(3)} = 3B_{xxxx} \int R(t)dt = 1.2 \times 10^{-10}\ \mathrm{cm}^3/\mathrm{erg}. \quad (4)$$

We then obtain for the delayed nonlinear index, $n_{2,d} = 12\pi^2 \chi^{(3)}/n_0^2 c = 5.1 \times 10^{-19}$ cm^2/W, close to previously published values of about 2×10^{-19} cm^2/W [26,28].

The fit in Fig. 4(a) was obtained using a lower nonlinear magnitude yielding $n_{2,d} = 2.5 \times 10^{-19}$ cm^2/W, also close to the accepted value. Despite being more intense, the filament-forming pulses in Fig. 4(a) exchanged the same percentage of energy as the weaker pulses of the same duration that did not form filaments (Fig. 2). This may be due to the intensity-clamping characteristic of filaments [29]. A detailed explanation will require full knowledge of the temporal and spatial pulse profiles at their intersection. Despite the complexity filament formation introduces to the interaction, the model predicts well the temporal dependence of the energy exchange for the positively chirped pulses. The model does not fit the negatively chirped pulse propagation, perhaps indicating a pulse affected by a higher degree of nonlinear propagation as the self-phase modulation partially counteracts the negatively chirped pulse profile. Nevertheless, that the interaction is robust in a variety of initial pulse chirps and energies indicates that TBC may be useful over a range of parameters.

In conclusion, we have shown that two intersecting filament-forming beams can experience an energy exchange of about 7%, controllable by adjusting their chirps and relative delay, and this in turn can affect filament propagation dynamics. Data obtained with positively-chirped beams were well reproduced using a model of the TBC process with impulsive stimulated Raman scattering as the delayed nonlinear component. Future experiments will concentrate on control of filament onset and length in collimated beams as well as the general amplification of chirped ultrashort pulses in the open air.

[1] A. Braun *et al.*, Opt. Lett. **20**, 73 (1995).
[2] C. P. Hauri *et al.*, Appl. Phys. B **79**, 673 (2004).
[3] X. M. Zhao *et al.*, IEEE J. Quantum Electron. **31**, 599 (1995).
[4] J. Kasparian *et al.*, Opt. Express **16**, 5757 (2008).
[5] P. Rairoux *et al.*, Appl. Phys. B **71**, 573 (2000).
[6] J. Kasparian *et al.*, Science **301**, 61 (2003).
[7] Z.-Y. Zheng *et al.*, Opt. Express **13**, 10616 (2005).
[8] J. Kasparian, R. Sauerbrey, and S. L. Chin, Appl. Phys. B **71**, 877 (2000).
[9] M. Kolesik, D. E. Roskey, and J. V. Moloney, Opt. Lett. **32**, 2753 (2007).
[10] G. Méchain *et al.*, Opt. Commun. **247**, 171 (2005).
[11] S. Eisenmann *et al.*, Opt. Express **15**, 2779 (2007).
[12] W. Jian, H. Cai, A. Couairon, and H Zeng (to be published).
[13] S. Varma, Y.-H. Chen, and H. M. Milchberg, Phys. Rev. Lett. **101**, 205001 (2008).
[14] H. J. Eichler, P. Günter, and D. W. Pohl, *Laser-Induced Dynamic Gratings*, Springer Series in Optical Sciences (Springer-Verlag, Berlin, 1986), Vol 50.
[15] S. A. Hosseini *et al.*, Phys. Rev. A **70**, 033802 (2004).
[16] A. Couairon *et al.*, Opt. Commun. **225**, 177 (2003).
[17] A. A. Ishaaya *et al.*, Phys. Rev. A **75**, 023813 (2007).
[18] T.-T. Xi, X. Lu, and J. Zhang, Phys. Rev. Lett. **96**, 025003 (2006).
[19] E. J. Brown, Q. Zhang, and M. Dantus, J. Chem. Phys. **110**, 5772 (1999).
[20] A. C. Bernstein *et al.*, Opt. Lett. **28**, 2354 (2003).
[21] T. A. Pitts *et al.*, J. Opt. Soc. Am. B **21**, 2008 (2004).
[22] A. Dogariu *et al.*, J. Opt. Soc. Am. B **14**, 796 (1997).
[23] S. Smolorz and F. Wise, J. Opt. Soc. Am. B **17**, 1636 (2000).
[24] W. Liu *et al.*, Opt. Lett. **30**, 2602 (2005).
[25] E. T. J. Nibbering *et al.*, Opt. Lett. **21**, 62 (1996).
[26] J. F. Ripoche *et al.*, Opt. Commun. **135**, 310 (1997).
[27] N. Tang and R. L. Sutherland, J. Opt. Soc. Am. B **14**, 3412 (1997).
[28] E. T. J. Nibbering *et al.*, J. Opt. Soc. Am. B **14**, 650 (1997).
[29] A. Becker *et al.*, Appl. Phys. B **73**, 287 (2001).